CHAPTER II
THEORETICAL BACKGROUND AND LITERATURE REVIEW

2.1 Diesel Fuel

Diesel fuel refers to a liquid fuel which is appropriate for compression ignition engines or diesel engines. Generally, diesel fuel is mainly referred to petroleum-based diesel but alternative non-petroleum-based diesel is increasingly being developed and adopted. Non-petroleum-based diesel refers to synthetic diesel, biodiesel and renewable diesel.

Synthetic diesel is diesel fuel that made by processing natural gas through a technology called the Fischer-Tropsch process, which converts the natural gas into synthetic diesel or gas-to-liquid (GTL). Synthetic diesel may also be produced out of biomass in the biomass-to-liquid (BTL) process or out of coal in the coal-to-liquid (CTL) process. Synthetic diesel has 30% lower particulate emissions than conventional diesel (US-California).

Biodiesel refers to any diesel-equivalent biofuel derived from vegetable oils or animal fats and other biomass-derived oils. Normally, biodiesel is defined as mono-alkyl ester. However, alkane (non-oxygenate) biodiesel is also available. The bio-based diesel-like hydrocarbon is called renewable diesel, green biodiesel or hydrogenated biodiesel.

In this section, the basic overviews of petroleum-based diesel and the more detail of bio-based diesel, biodiesel and renewable diesel which related to this work, in term of chemical reaction, processing condition and production process are described.

2.1.1 Petroleum-based Diesel

Petroleum diesel, also called petrodiesel or fossil diesel is produced from the fractional distillation of crude oil between 200 °C (392 °F) and 350 °C (662 °F) at atmospheric pressure, resulting in a mixture of carbon chains that typically contain between 8 and 21 carbon atoms per molecule. Normally, it is composed of

about 75% saturated hydrocarbons (primarily paraffins including *n*-, *iso*-, and cycloparaffins), and 25% aromatic hydrocarbons (including naphthalenes and alkylbenzenes). The average chemical formula for common diesel fuel is $C_{12}H_{23}$, ranging from approx. $C_{10}H_{20}$ to $C_{15}H_{28}$. Petroleum-based diesel is immiscible in water. It has the density of about 850 g/dm^3 and typically releases about 40.9 MJ/dm^3 when it is burnt.

2.1.2 Bio-based Diesel

Biodiesel is defined as any diesel-equivalent biofuel comprised of mono-alkyl esters of long chain fatty acids derived from vegetable oils or animal fats and other biomass-derived oils that meets the fuel specification requirements of the American Society of Testing and Materials (ASTM) D6751. In an article on proposed ASTM standards, biodiesel was defined as "the mono alkyl esters of long chain fatty acids derived from renewable lipid feedstock, such as vegetable oils or animal fats, for use in compression ignition (diesel) engines." Biodiesel can be used as a pure fuel (B100). Moreover, it can be blended with the conventional diesel. Biodiesel blends are denoted as "BXX" with "XX" representing the percentage of biodiesel contained in mixing process, such as B5 in Thailand, a blend of 5% biodiesel with 95% conventional diesel.

Renewable diesel is defined in the Internal Revenue Code (IRC) as diesel fuel produced from biological material using a process called "thermal depolymerization" that meets the registration requirements for fuels and fuel additives established by the Environmental Protection Agency (EPA) under section 211 of the Clean Air Act (42 U.S.C. 7545); and meets the requirements of the American Society of Testing and Materials (ASTM) D975 (petroleum diesel fuel) or D396 (home heating oil). Normally, renewable diesel is referred to hydrocarbons that do not contain oxygen in their molecular structure.

Thermal depolymerization is a process for the reduction of complex organic materials through the use of pressure and heat to decompose long-chain polymers of hydrogen, oxygen, and carbon into short-chain hydrocarbons with a

maximum length of around 18 carbon atoms. A process may qualify as thermal depolymerization even if catalysts are used in the process.

Biodiesel is produced from any triglyceride containing raw material. Vegetable oils and animal fats are considered as raw materials for biodiesel and renewable diesel production because they are widely available from a variety of sources, and they are renewable. The example of vegetable oils used for production are soybean oil, palm oil, sunflower oil, corn oil, jatropha oil, olive oil, canola oil, castor oil, coconut oil, cottonseed oil, etc. As well as recycled cooking oil, animal fats, trap grease (from restaurant grease traps), and float grease (from waste water treatment plants), are also available as raw materials for biodiesel and renewable diesel production. These products, when compared to plant-derived oils, often offer an economical advantage as a feedstock. There is also some indication that these sources, which are high in saturated fats, produce less nitrous oxide compared to plant-derived oils.

Both oils and fats consist of molecules called triglycerides. Fat generally refers to the triglycerides in solid form at room temperature, whereas oils are liquid at room temperature. The molecule of triglyceride is composed of three long-chain fatty acids of 8 to 22 carbons attached to a glycerol backbone. Figure 2.1 shows the chemical structure of a triglyceride, where R1, R2, and R3, which may be the same or different, represent long chain fatty acids, which are mostly palmitic, stearic, oleic, linoleic, and linolenic acids. Fatty acid composition of some common edible fat and oil (Zamora, 2005) as shown in Table 2.1. Vegetable oils contain free fatty acids (generally 1-5 %), carotenes, phosphatides, phospholipids, sulphur, tocopherols compounds, and traces of water.

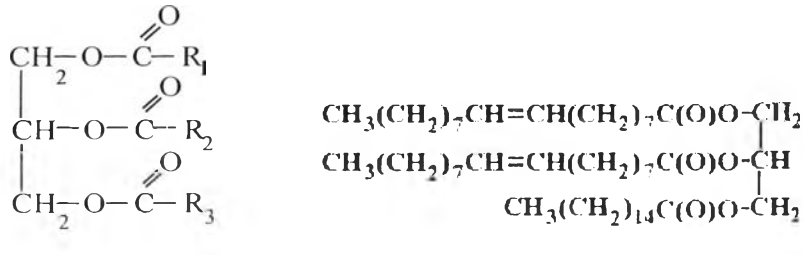

Figure 2.1 A chemical structure of triglyceride.

Table 2.1 Fatty acid composition of some common edible fat and oil (Zamora, 2005)

Oil or Fat	Unsat./Sat. ratio	Saturated					Mono unsaturated	Poly unsaturated	
		Capric Acid	Lauric Acid	Myristic Acid	Palmitic Acid	Stearic Acid	Oleic Acid	Linoleic Acid (ω6)	Alpha Linolenic Acid (ω3)
		C10:0	C12:0	C14:0	C16:0	C18:0	C18:1	C18:2	C18:3
Almond Oil	9.7	-	-	-	7	2	69	17	-
Beef Tallow	0.9	-	-	3	24	19	43	3	1
Canola Oil	15.7	-	-	-	4	2	62	22	10
Cocoa Butter	0.6	-	-	-	25	38	32	3	-
Cod Liver Oil	2.9	-	-	8	17	-	22	5	-
Coconut Oil	0.1	6	47	18	9	3	6	2	-
Corn Oil	6.7	-	-	-	11	2	28	58	1
Cottonseed Oil	2.8	-	-	1	22	3	19	54	1
Flaxseed Oil	9.0	-	-	-	3	7	21	16	53
Grape seed Oil	7.3	-	-	-	8	4	15	73	-
Lard (Pork fat)	1.2	-	-	2	26	14	44	10	-
Olive Oil	4.6	-	-	-	13	3	71	10	1
Palm Oil	1.0	-	-	1	45	4	40	10	-
Palm Olein	1.3	-	-	1	37	4	46	11	-
Palm Kernel Oil	0.2	4	48	16	8	3	15	2	-
Peanut Oil	4.0	-	-	-	11	2	48	32	-
Sesame Oil	6.6	-	-	-	9	4	41	45	-
Soybean Oil	5.7	-	-	-	11	4	24	54	7
Sunflower Oil	7.3	-	-	-	7	5	19	68	1
Walnut Oil	5.3	-	-	-	11	5	28	51	5

Note Percent by weight of total fatty acid

2.1.2.1 Biodiesel

Biodiesel refers to any diesel-equivalent biofuel derived from vegetable oils or animal fats and other biomass-derived oils. Normally, biodiesel is defined as mono-alkyl ester which is a liquid varies in color, golden to dark brown, depending on type of feedstock. It is immiscible in water. Most of mono-alkyl ester has high boiling point (in the range of 620-630 K) and low vapor pressure (less than 1 mm Hg). Its flash point is higher than 130 °C, significantly higher than that of the conventional diesel (64 °C), and its density is in the range of 0.86 to 0.90 g/cm^3, less than the density of water. The production of biodiesel from bio-oils is a chemical reaction called transesterification.

Biodiesel, which is referred to mono-alkyl ester, is normally produced via the transesterification of vegetable oils or animal fats (triglycerides). In this process, triglycerides react with alcohols, generally methanol or ethanol, in the presence of a catalyst to produce mono-alkyl esters and glycerol. The transesterification reaction can be catalyzed by bases, acids, or enzymes with minimal side reactions and reaction time, and are a direct conversion to biodiesel with no intermediate compounds. The most common catalysts used are strong bases, such as sodium hydroxide, potassium hydroxide, and sodium methoxide. The major components of biodiesel are straight-chain fatty acids, and the most common ones contain 16 and 18 carbon atoms. The typical transesterification process is shown in Figure 2.2.

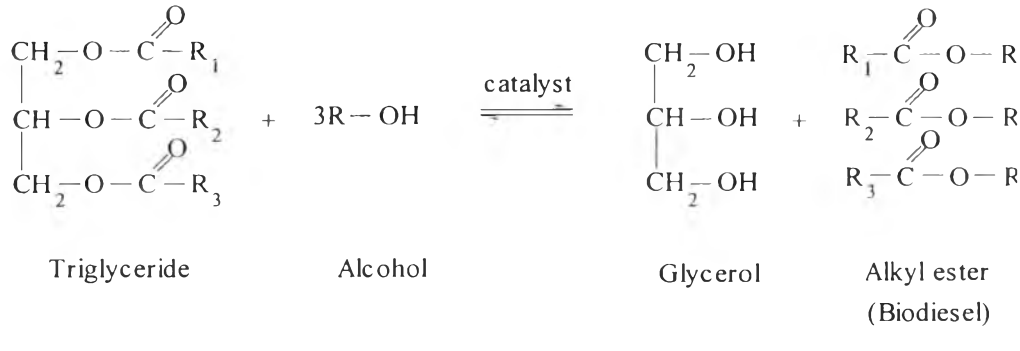

Figure 2.2 The production of biodiesel via transesterification of triglyceride (Srivastava *et al.*, 2000).

The stoichiometric relation between triglyceride and alcohol is a one mole of triglyceride reacting with three moles of alcohol. However, for transesterification to occur, usually 6 moles of alcohol are used for every mole of triglyceride, which is more than the equation indicated. The reason is that the equilibrium of the reaction needs to be shifted toward the right side of the equation. To force the equilibrium in the direction of the desired products, one or more parameter(s) of the reaction may need to be changed, such as the molar ratio, temperature, pressure, and catalyst type.

The overall process of transesterification is shown in Figure 2.3. It is normally three consecutive steps, which are reversible reactions.

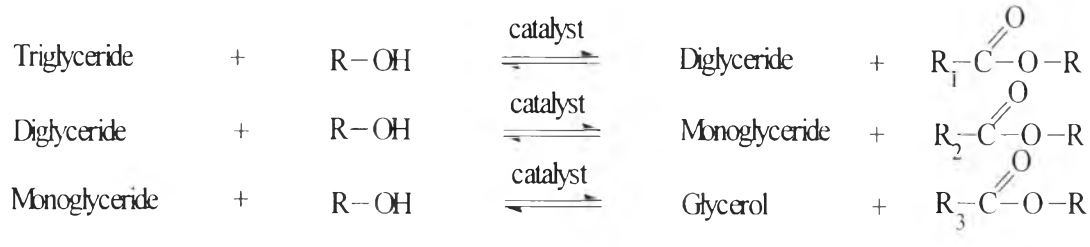

Figure 2.3 The transesterification reactions of triglyceride with alcohol to ester and glycerol (Srivastava *et al.*, 2000).

Figure 2.4 shows the simple reaction of triglyceride with methanol, resulting in the most popular mono-alkyl ester, which is methyl ester.

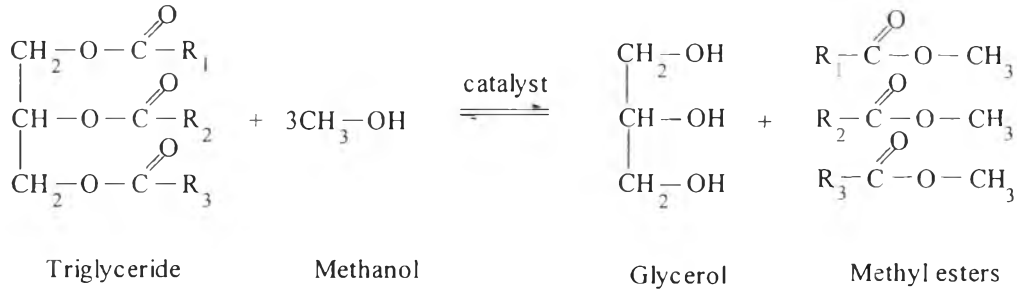

Figure 2.4 The transesterification reactions of triglyceride with methanol (Srivastava *et al.*, 2000).

The conversion of triglycerides into mono-alkyl esters through the transesterification reaction reduces the molecular weight to one-third that of the triglyceride and slightly increases the volatility.

Although mono-alkyl ester is considered as a potential sustainable alternative fuel but there are still disadvantages associated with its use. There are several properties of mono-alkyl ester that limit their uses. First, mono-alkyl ester has cloud point and pour point higher than conventional diesel, the performance of biodiesel in cold conditions is poorer than petroleum diesel, which might be caused engine problems and increased nitrogen oxide emissions (Xue, *et al.*, 2011). Biodiesel has been shown to increase nitrogen oxide (NO_x) emissions in many engines on engine stand tests. Biodiesel does not contain nitrogen so the increasing NO_x phenomenon is not related to fuel nitrogen content. NO_x is created in the engine as the nitrogen in the intake air reacts with oxygen at the high in-cylinder combustion temperatures (Fazal, *et al.*, 2011, Hoekman, *et al.*, 2012). Second, mono-alkyl ester is a good solvent, it can dissolve rubber and some plastics, remove paint, and oxidize the metals. Third, the hydrophilic property of mono-alkyl ester might cause the corrosion of the engine. Lastly, mono-alkyl ester contains oxygen which may be undesirable for certain applications. The presence of oxygen lowers the heat content as shown by the volumetric heating values of it, which are 9-13% lower than conventional diesel (Demirbar, 2003). Moreover, this production route has several economic considerations mainly attributed to the price and availability of the main byproduct glycerin. Another drawback is the demand for large biodiesel production units requiring large investments (Knothe *et al.*, 2005).

Therefore, the deoxygenation of triglyceride becomes an alternative process of renewable diesel production because there are a lot of advantages of this process over transesterification, including compatibility with infrastructure, engines and fuel standards, lower processing costs and raw materials flexibility (Stumborg *et al.*, 1996). Moreover, the obtain products from this process have high quality and have similar property to the conventional diesel fuel.

2.1.2.2 Renewable Diesel

Renewable diesel can be produced via hydrotreating which is another route to produce of renewable diesel or renewable liquid alkane substitute from vegetable oils and fats, which contain the triglyceride, as shown in Figure 2.5. The standard hydrotreating conditions are 300-450 °C with conventional hydrotreating catalysts (i.e. NiMo/γ-Al_2O_3, sulfided NiMo/γ-Al_2O_3, Pd/C). In hydrotreating process, the hydrocarbons are produced by the three difference pathways: (i) hydrodeoxygenation (or dehydration/ hydrogenation), (ii) hydrodecarboxylation, and (iii) hydrodecarbonylation. In hydrodeoxygenation reaction, the hydrocarbon chain is broken, and undesired oxygen is removed, leading to a production of straight-chain hydrocarbons suitable for diesel fuel. The normal alkanes originating from HDO have the same carbon number as the original fatty acid chain, i.e. even carbon number, typically 16 or 18.

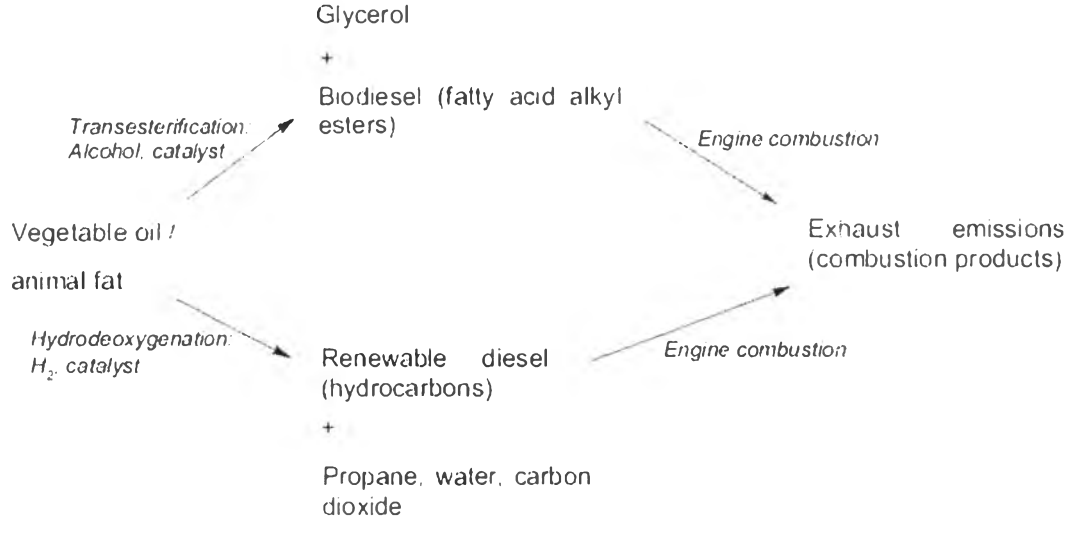

Figure 2.5 Flowchart for transformation of lipid materials (biodiesel and renewable diesel by hydrodeoxygenation) to products of engine combustion (Knothe, 2010).

Renewable liquid alkanes or renewable diesel can be produced by hydrotreating of vegetable oils at standard hydrotreating conditions (i.e. 300-450 °C) with conventional hydrotreating catalysts (sulfided NiMo/Al_2O_3, NiMo/γ-Al_2O_3). Huber *et al.*, (2007) studied hydrotreating of pure sunflower oil in a fixed bed reactor

with a sulfided NiMo/γ-Al_2O_3 catalyst. The reaction was done at temperature ranging from 300 to 450 °C, pressure of 50 bar, LHSV 4.97 h^{-1} and H_2 to feed ratio of 1600 ml H_2 /ml liquid feed. The products obtained were analyzed by GC. It was found that the fraction distilled from 250 to 350 °C was the major distillation fraction. This fraction is mostly n-C15, n-C16, n-C17, and n-C18. The mixture in this fraction occurred at reaction temperature of 350 °C. The reaction pathways involves hydrogenation of the C=C bonds of the vegetable oils followed by alkane production by three different pathways: decarbonylation, decarboxylation and hydrodeoxygenation as shown in Figure 2.6. Moreover, the straight chain alkanes can undergo isomerization and cracking to produce lighter and isomerized alkanes. In addition, they proposed that the catalyst and reaction condition play an important role to determine the yield of the decarbonylation, decarboxylation and hydrodeoxygenation pathways.

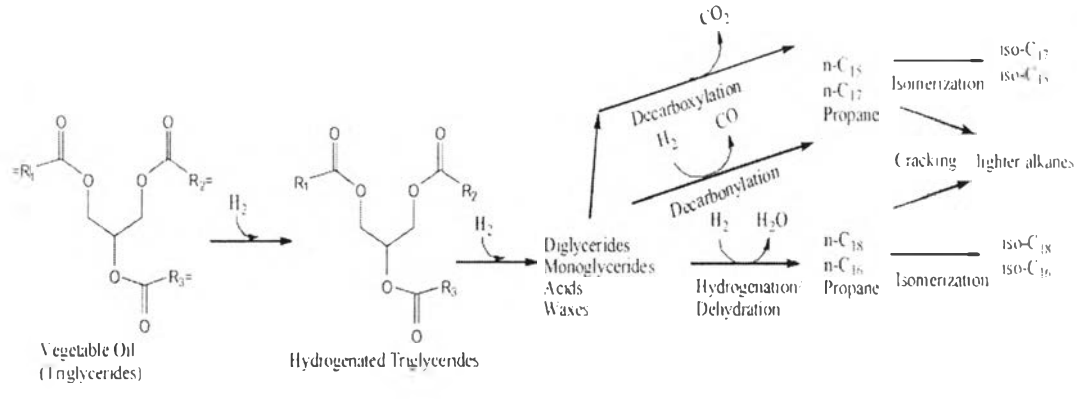

Figure 2.6 The reaction pathway for conversion of triglycerides to renewable diesel (Huber *et al.*, 2007).

In the first step of this reaction pathway the triglyceride is hydrogenated and broken down into various intermediates which are monoglycerides, diglycerides and carboxylic acids. These intermediates are then converted into alkanes by three different pathways: decarboxylation, decarbonylation and hydrodexogenation (or dehydration/hydrogenation). Moreover, the straight chain alkanes can undergo isomerization and cracking to produce lighter and isomerized alkanes. In addition, they proposed that the catalyst and reaction condition play an

important role to determine the yield of the decarbonylation, decarboxylation and hydrodeoxygenation pathways.

There are several possible reaction pathways for a production of straight-chain hydrocarbons, shown as Figure 2.7. Carboxylic acids have used to represent feedstock and similar equations can be written for alkane production from mono-, di- or tri-glycerides. Fatty acids can be directly decarboxylated or decarbonylated. Direct decarboxylation removes the undesired oxygen by releasing carbon dioxide and producing aliphatic hydrocarbon chains with one carbon atom less than in the original feed, while direct decarbonylation removes the undesired oxygen by forming carbon monoxide and water, as explained by reactions I and II. Moreover, the fatty acid can be deoxygenated by adding hydrogen leading to a production of straight-chain hydrocarbons and undesired oxygen will be removed through formation of water, as explained by reactions III (Snare *et al.*, 2006). This pathway involves bifunctional catalysis that contains sites for hydrogenation reactions (possibly NiMo sites) and for dehydration reactions (acid catalytic sites). It is possible that the free fatty acid intermediates are catalyzing the dehydration reaction. The hydrogen requirements decreases as hydrodeoxygenation > decarbonylation pathway > decarboxylation pathway. (Huber *et al.*, 2007)

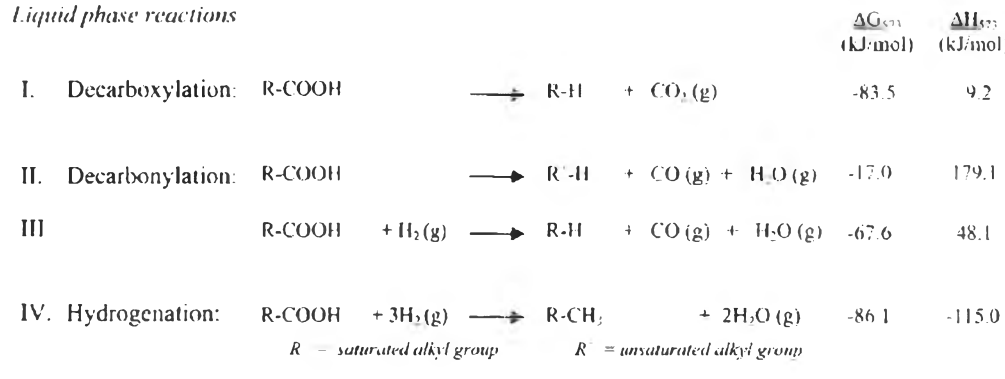

Figure 2.7 The possible liquid-phase reaction pathways for production of straight-chain hydrocarbons from fatty acids. (Snare *et al.*, 2006)

In addition to the liquid-phase reactions, the water gas shift and methanation reaction are occurred with a number of carbon monoxide, carbon dioxide, hydrogen, and water formed during decarbonylation/decarboxylation reaction. The water-gas-shift reaction may balance the concentrations of CO and CO_2, while methanation reaction of fatty acids gives methane and water, shown as Figure 2.8.

Gas phase reactions								ΔG_{573} (kJ/mol)	ΔH_{573} (kJ/mol)
V. Methanation:	CO_2	+	$4H_2$	$\rightleftharpoons$	CH_4	+	$2H_2O$	-61.2	-177.2
VI. Methanation:	CO	+	$3H_2$	$\rightleftharpoons$	CH_4	+	H_2O	-78.8	-216.4
VII. Water-gas-shift	CO	+	H_2O	$\rightleftharpoons$	H_2	+	CO_2	17.6	-39.2

Figure 2.8 Gas phase reactions of CO or CO_2 with H_2 or H_2O.(snare *et al.*,2006)

Snare *et al.*, (2006) investigated the deoxygenation of stearic acid over the heterogeneous catalysts for production of biodiesel. A variety of metal (Pd, Pt, Ru, Mo, Ni, Rh, Ir, and Os) supported on Al_2O_3, Cr_2O_3, MgO, and SiO_2, as well as activated carbons were studied by using stearic acid as a model compound. The deoxygenation reaction is carried out in a semibatch reactor under constant temperature and pressure, 300 °C and 6 bar, respectively. In case of noncatalytic deoxygenation, it was found that less than 5% of stearic acid was convertedwithin 6 h of reaction and the main products formed were linear C17 hydrocarbons. In the heterogeneous catalytic deoxygenation of stearic acid achieved with high activity and selectivityto n-heptadecane (n-C17). The catalyst screening showed that the reaction can be effectively performed over palladium and platinum supported on activated carbons. Furthermore, the gas phase analysis indicated that the decarboxylation reaction was more preferably over the Pd/C catalyst, as the decarbonylation was more preferably over the Pt/C catalyst.

In 2009, Nontawong *et al.* studied the conditions for the production of hydrogenated biodiesel from vegetable oil i.e. palm oil and jatropha oil over $NiMo/Al_2O_3$ and Pd/C catalysts under various temperatures, pressures, H_2/feed

molar ratios, and liquid hourly space velocities. The results showed that the suitable conditions were 325 °C, 500 psig, and H_2 to feed molar ratio of 30. Palm oil can be hydrodeoxygenated to paraffinic hydrocarbons that have carbon atom in diesel specification range (C15 to C18 hydrocarbons) over both $NiMo/Al_2O_3$ and Pd/C catalysts under moderate conditions. Over the $NiMo/Al_2O_3$ catalyst, palm oil was converted with high selectivity to long chain alkanes with carbon atoms equivalent to the carbon atoms of fatty acids in each oil molecule that are n-octadecane (n-C18) and n-hexadecane (n-C16), indicates that the deoxygenation of palm oil over the $NiMo/Al_2O_3$ prefer to occur via hydrodeoxygenation. In case of the Pd/C catalyst, major fraction from palm oils are n-heptadecane (n-C17) and n-pentadecane (n-C15), alkane products that have one carbon atom less than the original fatty acids in each oil molecule, indicates that the deoxygenation of palm oil over the Pd/C tends to undergo hydrodecarbonylation pathway.

Chinsutthi *et al.*, (2010) investigated the effect of catalyst supports on the deoxygenation of beef fat for the production of hydrogenated biodiesel over Pd-based catalysts (i.e. Pd/Al_2O_3, $Pd/F\text{-}Al_2O_3$, Pd/SiO_2, Pd/TiO_2, Pd/C, and Pd/KL) and NiMo-based catalysts (i.e. $NiMo/Al_2O_3$, $NiMo/F\text{-}Al_2O_3$, $NiMo/SiO_2$, $NiMo/TiO_2$, NiMo/C, and $NiMo/CeO_2\text{-}ZrO_2$). The catalysts were tested in a continuous flow packed-bed reactor at 500 psig, 325 °C, H_2/feed molar ratio of 30, and LHSV 1 h^{-1}. The different catalysts gave the different conversions and product distributions. There were two main groups of liquid products which were hydrocarbons and oxygenate (fatty acids, fatty alcohols, and fatty esters). The results showed that hydrocarbons obtained from all catalysts were in the range of diesel fuel. The catalysts support affected the catalyst surface area, metal dispersion, but not the reaction pathway. The main hydrocarbons product obtained over all Pd catalysts were n-heptadecane (n-C17) and n-pentadecane (n-C15), resulting from hydrodecarbonylation. On the other hand, the main hydrocarbons product obtained over all NiMo catalysts were mainly n-octadecane (n-C18) and n-hexadecane (n-C16), resulting from hydrodeoxygenation. Among Pd supported catalysts, Pd/TiO_2 gave the highest hydrocarbon yield and conversion, due to the high dispersion of Pd on TiO_2 support.

2.2 Titanium dioxide (TiO_2)

2.2.1 General Remarks

Titanium dioxide (TiO_2) belongs to the family of transition metal oxides. In the beginning of the 20th century, industrial production started with titanium dioxide replacing toxic lead oxides as pigments for white paint. At present, the annual production of TiO_2 exceeds 4 million tons. It is used as a white pigment in paints (51% of total production), plastic (19%), and paper (17%), which represent the major end-use sectors of TiO_2. The consumption of TiO_2 as a pigment increased in the last few years in a number of minor end-use sectors such as textiles, leather, pharmaceuticals and various titanate pigments (mixed oxides). (Carp *et al.*, 2004)

Titanium dioxide has attracted tremendous attention from researchers worldwide due to its chemical stability, non-toxicity, low cost, and other advantageous properties. As a result of its high refractive index, it is used as anti-reflection coating in silicon solar cells and in many thin-film optical devices. TiO_2 is successfully used as gas sensor due to the dependence of the electric conductivity on the ambient gas composition and is utilized in the determination of oxygen and CO concentrations at high temperatures (> 600 °C), and simultaneously determining CO/O_2 and CO/CH_4 concentrations. Moreover, due to its hemocompatibility with the human body, TiO_2 is used as a biomaterial (as bone substituent and reinforcing mechanical supports)

TiO_2 is also used in catalytic reactions acting as a promoter, a carrier for metals and metal oxides, an additive, or as a catalyst. Reactions carried out with TiO_2 catalysts include selective reduction of NO_x to N_2, effective decomposition of VOCs, hydrogen production by gas shift production, Fischer–Tropsch synthesis, CO oxidation by O_2, H_2S oxidation to S, reduction of SO_2 to S by CO, and NO_2 storage.

Rutile is investigated as a dielectric gate material for MOSFET devices as a result of its high dielectric constant (e > 100) and doped anatase films (using Co) might be used as a ferromagnetic material in spintronics. In batteries, the anatase form is used as an anode material in which lithium ions can intercalate reversibly. For solar cell applications, the anatase structure is preferred over the

rutile structure, as anatase exhibits a higher electron mobility, lower dielectric constant, lower density, and lower deposition temperature.

2.2.2 Crystal Structure and Properties

The main four polymorphs of TiO_2 found in nature are anatase (tetragonal), brookite (orthorhombic), rutile (tetragonal), and TiO_2 (B) (monoclinic). The structures of rutile, anatase and brookite can be discussed in terms of (TiO_2^{6-}) octahedrals. The three crystal structures differ by the distortion of each octahedral and by the assembly patterns of the octahedral chains. Anatase can be regarded to be builtup from octahedrals that are connected by their vertices, in rutile, the edges are connected, and in brookite, both vertices and edges are connected, as shown in Figure 2.9.

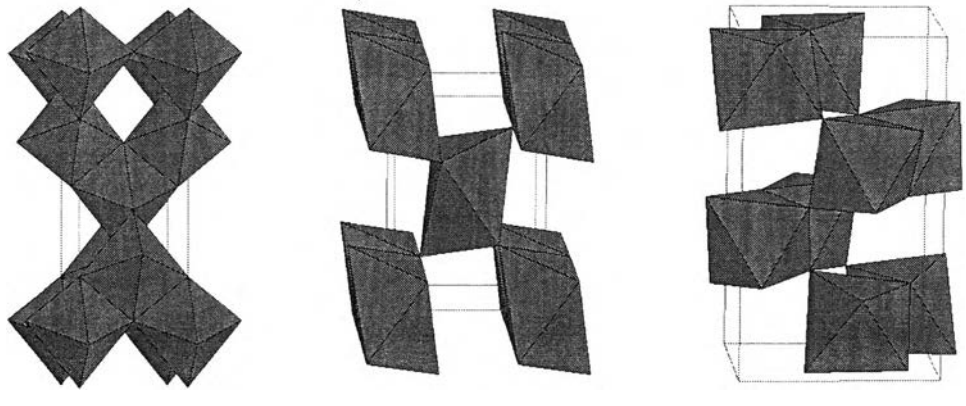

(a) (b) (c)

Figure 2.9 Crystal structures of (a) anatase, (b) rutile, and (c) brookite (carp et al., 2004)

2.2.3 Synthesis and Morphologies

TiO_2 can be prepared in the form of powder, crystals, or thin films. Both powders and films can be built up from crystallites ranging from a few nanometers to several micrometers. It should be noted that nanosized crystallites tend to agglomerate. If separate nanosized particles are desired, often a

deagglomeration step is necessary. Many novel methods lead to nanoparticles without an additional deagglomeration step.

2.2.3.1 Solution Routes

For some applications, especially the synthesis of thin films, liquid-phase processing is one of the most convenient and utilized methods of synthesis. This method has the advantage of control over the stoichiometry, producing homogeneous materials, allowing formation of complex shapes, and preparation of composite materials. However, there are several disadvantages for example expensive precursors, long processing times, and the presence of carbon as an impurity. The most commonly used solution routes in the synthesis of TiO_2 are:

a) Precipitation (co-)methods. These involve precipitation of hydroxides by the addition of a basic solution (NaOH, NH_4OH, urea) to a raw material followed by calcination to crystallize the oxide.

b) Solvothermal methods. These methods employ chemical reactions in aqueous (hydrothermal method) or organic media (solvothermal method) such as methanol, 1,4 butanol, toluene under self-produced pressures at low temperatures (usually under 250 °C).

c) Sol–gel methods. These methods are used for the synthesis of thin films, powders, and membranes. Two types are known: the non-alkoxide and the alkoxide route. The sol–gel method has many advantages over other fabrication techniques such as purity, homogeneity, felicity and flexibility in introducing dopants in large concentrations, stoichiometry control, ease of processing, control over the composition, and the ability to coat large and complex areas.

d) Microemulsion methods. Water in oil microemulsion has been successfully utilized for the synthesis of nanoparticles.

e) Combustion synthesis. Combustion synthesis (hyperbolic reaction) leads to highly crystalline fine/large area particles. The synthetic process involves a rapid heating of a solution/compound containing redox mixtures/redox groups.

f) Electrochemical synthesis. Electrochemical synthesis may be used to prepare advanced thin films such as epitaxial, superlattice, quantum dot and nanoporous ones.

2.2.3.2 Gas Phase Methods

For thin films, most synthesis routes are performed from the gas phase. These can be chemical or physical of nature. Most of these techniques can also synthesize powder, if a method to collect the produced particles is employed. The main techniques are:

a) Chemical vapour deposition (CVD). CVD is a widely used versatile technique to coat large surface areas in a short span of time. In industry, this technique is often employed in a continuous process to produce ceramic and semiconductor films.

b) Physical vapour deposition (PVD). PVD is another class of thin film deposition techniques. Films are formed from the gas phase, but here without a chemical transition from precursor to product. This is, therefore, only possible with substances that are stable in the gas phase and can be directed towards the substrate.

c) Spray pyrolysis deposition (SPD). SPD is an aerosol deposition technique for thin films and powders related to CVD. The main differences are that in spray pyrolysis:

(1) an aerosol (a mist of small droplets) is formed from a precursor solution instead of a vapour in CVD.

(2) the aerosol is directly focussed onto the sample in most cases, whereas diffusion is a dominant process in CVD.

d) Other method: Sputtering, Molecular beam epitaxy, Ion implantation and dynamic ion beam mixing.

TiO_2 is also synthesized in special morphologies. Nanostructures especially have been built in various sizes and shapes. To complete the list, we include: nanorods, platelets, nanowires, nanowalls, nanotubes, nanoribbons,

whiskers, inverse opals (ordered mesoporous materials in which air voids are surrounded by TiO_2 in a 3-D lattice), and fractals as shown in Figure 2.10.

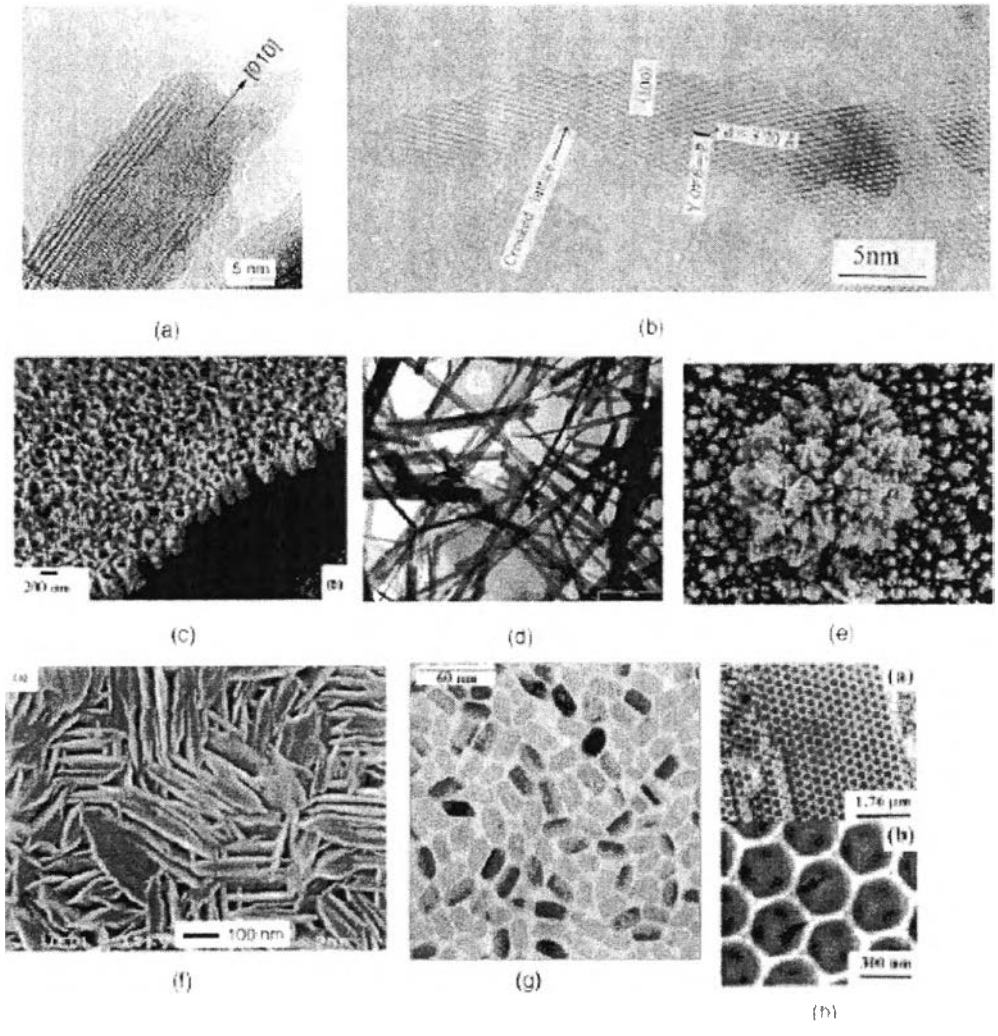

Figure 2.10 Morphologies of nanosized TiO_2 (Carp *et al.*, 2004)

(a) nanorods (b) platelets (c) nanowires (d) nanowalls

(e) nanotubes (f) nanoribbons (g) whiskers (h) inverse opals

In addition, some of the most important bulk properties of TiO_2 are presented in Table 2.3.

Table 2.2 Some bulk properties of the three main polymorphs of TiO_2 (anatase, rutile, and brookite) (Carp *et al.*, 2004)

Crystal structure	**System**	**Space group**	**Lattice constants (nm)**			
			A	**b**	**c**	**c/a**
Rutile	Tetragonal	D_{4h}^{14}-$P4_2/mmm$	0.46	-	0.29	0.64
Anatase	Tetragonal	D_{4h}^{19}-$I4_1/amd$	0.37	-	0.94	2.51
Brookite	Rhombohedral	D_{2h}^{15}-Pbca	0.54	0.92	-	0.94
Density (kg/m^3)						
Rutile			4240			
Anatase			3830			
Brookite			4170			
Dielectric properties	Frequency (Hz)	Temperature (K)	Dielectric constant			
Rutile, perpendicular to optical c-axis	10^8	290-295	86			
Rutile, parallel to optical c-axis	-	290-295	170			
Rutile, perpendicular to optical c-axis	10^4	298	160			
Rutile, along c-axis	10^7	303	100			
Anatase, average	10^4	298	55			
Band gap (eV)						
Rutile			3.05			
Anatase			3.26			
Refractive index	n_g	n_p				
Rutile	2.95	2.65				
Anatase	2.57	2.66				
Brookite	2.80	2.68				

2.3 Sol-Gel Process

The sol–gel process involves first the formation of a sol followed by that of a gel. A sol, which is a liquid suspension of solid particles ranging in size from 1 nm to 1 micron, can be obtained by the hydrolysis and partial condensation of a precursor, such as an inorganic salt or a metal alkoxide. The further condensation of sol particles into a three-dimensional network produces a gel, which is a material with a solid encapsulating a solvent. Alternatively, a gel can be produced by destabilizing a solution of preformed sols. In either case, the materials are referred to aquasol (or aquagel) when water is used as a solvent, and alcosol (or alcogel) when alcohol is used. The encapsulated liquid can be removed from a gel by either evaporative drying or drying with supercritical extraction (supercritical drying for short). The resulting solid products are known as a xerogel and an aerogel, respectively. (Ertl *et al.*,1997)

The single most important characteristic of the sol-gel preparation of catalyst material is its ease of control that translates into the following advantages:

(i) the ability to maintain high purity (because of purity of the starting materials);

(ii) the ability to change physical characteristics such as pore size distribution and pore volume;

(iii) the ability to vary compositional homogeneity at a molecular level;

(iv) the ability to prepare samples at low temperature;

(v) the ability to introduce several components in a single step;

(vi) the ability to produce samples in different physical forms.

Figure 2.11 shows the four key steps in taking a precursor to a particular product form via sol-gel preparation: formation of a gel, aging of a gel, removal of solvent, and heat treatment.

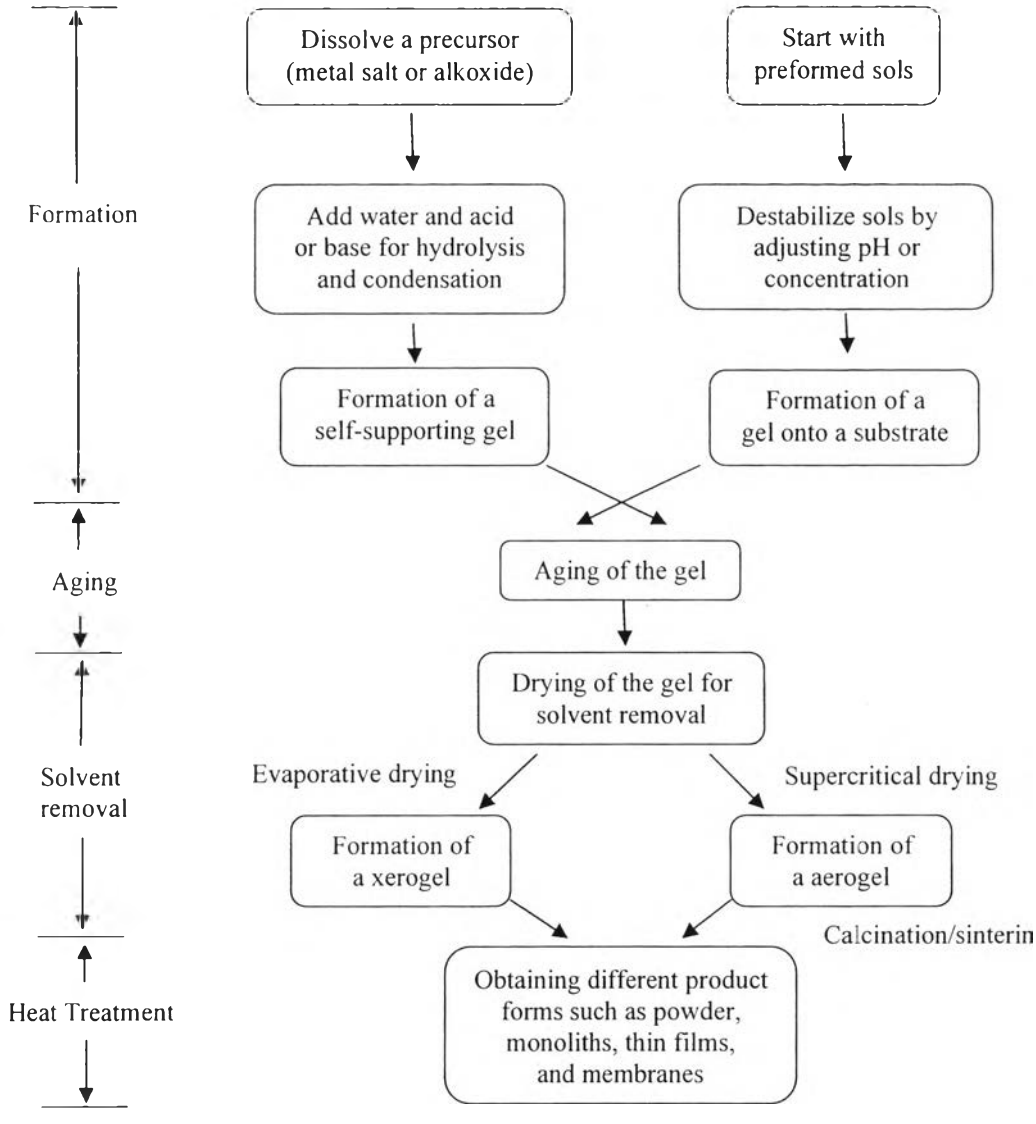

Figure 2.11 Schematic diagram showing the various steps of a sol-gel process (Ertl *et al.*,1997)

The precursor in a sol–gel preparation can either be a metal salt/alkoxide dissolved in an appropriate solvent or a stable colloidal suspension of preformed sols. Metal alkoxides have been the most extensively used because they are commercially available in high purity, and their solution chemistry has been documented. At its simplest level, sol-gel chemistry with metal alkoxides can be described in terms of two classes of reactions:

Hydrolysis: $-M-OR + H_2O \rightarrow -M-OH + ROH$

Condensation: $-M-OH + X-OM- \rightarrow -M-O-M + XOH$

where X can either be H or R (an alkyl group)

Su *et al.* (2004) studied titanium dioxide preparation by using sol-gel method that is one of the most successful techniques for preparing nanosized metallic oxide materials with high photocatalytic activities. In sol-gel processes, TiO_2 is usually prepared by the reactions of hydrolysis and polycondensation. A solution of titanium (IV) n-butoxide ($Ti(O\text{-}Bu)_4$,) in isopropyl alcohol (i-PrOH), was used as molecular precursor of TiO_2. Moreover, acetylacetone (acac) was used as a chemical additive to moderate the reaction rate. The molar ratio of these reactants was: $Ti(OBu)_4$:H_2O:i-PropOH:acac = 1:100:2:0.01. The final solution was peptized to give a sol of pH~2.5. The other portion was gelled by drying at 100 °C for 3 h, then calcinated in vacuum oven at various temperatures (400–700 °C) to give TiO_2 powder. The XRD patterns as shown in Table 2.4 showed that the amorphous phase crystallizes to the anatase structure at temperature of 400 °C. However, when the TiO_2 was heated up to 500 °C and above, the products became a mixture of anatase and rutile. The results revealed that increasing of the calcination temperature accelerates phase transformation from thermodynamically metastable anatase to most stable and more condense rutile phase. From BET results as shown in Table 2.5, the specific surface area shift towards smaller values at higher calcination temperatures. The observation indicates that increasing of the crystal size and decreasing of the surface area are the result of increasing of the calcination temperature.

Table 2.3 Results of XRD measurements for TiO_2 samples (Su *et al.*,2004)

Calcination temperature (T_c) (°C)	Diffraction angle (2θ)	FWHM (radian)	Crystal size (nm)	A/R
Before annealing (A)	25.55	0.037520	4.10	
400 (A)	25.64	0.011010	13.96	9.8
500 (A)	25.65	0.008740	17.60	3.23
500 (R)	27.51	0.008323	18.78	
600 (A)	25.46	0.007426	20.68	0.12
600 (R)	27.51	0.005941	26.31	
700 (A)	25.56	0.005812	26.44	0.03
700 (R)	27.44	0.004455	35.07	

Table 2.4 Surface area of TiO_2 samples (Su *et al.*,2004)

Calcination temperature(°C)	Surface area (m^2g^{-1})
400	122.2
500	65.7
600	26.9
700	11.5
800	52.0

In addition, the degradation of salicylic acid was selected as a test reaction to verify the photocatalytic activity of different TiO_2 dispersion samples. The results showed that TiO_2 catalyst calcined at 500 °C is the most active to catalyze the photodecomposition of salicylic acid. On the other hand, the TiO_2 catalyst calcined at 700 °C showed only little photocatalysis efficiency to decompose salicylic acid. It may be due to the phase transformation from anatase which is usually believed to be more photocatalytically active to rutile after high temperature calcinations. Furthermore, the TiO_2 catalyst calcined at 400 °C exhibited lower

photocatalysis efficiency than that of the TiO_2 catalyst calcined at 500 °C even though it possessed the largest surface area and it is composed primarily of anatase phase. From the XRD patterns, they indicated that anatase crystallization of TiO_2 treated at 400 °C was incomplete. The amorphous titania have very low photocatalytic efficiency compared to that of the anatase or rutile phase due to an increased electron-hole recombination rate.

In 2004, Sukulkhaemaruethai *et al.* studied on the effect of processing variations on the structural and morphological characteristics (e.g. phase transformation, particle size, surface area) and photocatalytic activity of titania nanocrystals prepared via surfactant-assisted templaing method (SATM) using tetra (i-propyl) orthotitanate (TIPT) modified with acetylacetone (ACA) in the presence of laurylamine hydrochloride (LAHC) as templating agent compared with ST-01 commercial titania nanomaterials. The effect of parameter including the surfactant-removing process, surfactant to alkoxide ratio, ACA concentration, pH value, and water to alkoxide ratio on the material properties of titania nanocrystal has been investigated and they found that the mesoporous titania nanocrystals exhibit mesoporous anatase-type structure with S_{BET} up to 140 m^2/g under the optimum condition of [ACA]/[TIPT]=1, [LAHC]/[TIPT]=0.25 pH 4.5, with alcohol washing and calcined at 500 °C and the synthesized mesoporous titania nanocrystals show higher photocatalytic activity than of that ST-10.

Nanocrystalline mesoporous titania synthesized via a combined sol–gel process with surfactant-assisted templating method was studied by Sreethawong *et a*l. in 2004. They concentrated on the effect of calcination conditions and evaluated for its photocatalytic activity through photocatalytic hydrogen evolution from an aqueous methanol solution. TIPT was used as a titanium precursor for mesoporous TiO_2 photocatalyst. LAHC was used as a template behaving as a mesopore forming agent and a gel formation-assisting agent and ACA serves as a modifying ligand, was applied to moderate the hydrolysis and condensation processes of titanium precursor species. TiO_2 catalyst prepared by sol-gel method was compared with commercially available TiO_2 powders, Ishihara ST-01 and Degussa P-25 in comparative study of photocatalytic H_2 evolution. ACA was introduced into TIPT with the same mole and the molar ratio of TIPT to LAHC of

pH 4.2 was tailored to the value of 4. The samples were calcined at 500-700 °C for 1-24 h.

From the TG-DTA results, the DTA curve shows two main exothermic peaks. The first exothermic peak, with its maximum at 334.4 °C is attributed to the burnout of the surfactant template. The second exothermic peak, with its maximum at 438.3 °C, corresponds to the crystallization process of the photocatalyst. The XRD patterns of the samples calcined at 500 and 600 °C for entire calcination time showed crystalline structure of pure anatase phase. Nevertheless, the crystallization to anatase phase at 500 °C of the synthesized materials was not fully developed even at calcination time of 24 h. The calcination temperature of 600 °C was determined as the highest limit for yielding well-crystallized pure anatase phase TiO_2. Besides, at 700 °C calcinations, partial phase transformation from anatase to rutile was observed, resulting in the combination of anatase and rutile phases. From the experimental results on BET surface area, mean pore diameter, and total pore volume, showed that the surface area decreased with both calcination time and temperature due to pore coalescence that caused an increase in mean pore diameter and a decrease in total pore volume of the bulk materials.

Among these three calcination temperatures, H_2 evolution activity reached the maximum value at calcination temperature of 600 °C for the entire range of calcination time. Although surface area of the materials calcined at 600 °C was smaller than that at 500 °C, perfect crystallization of anatase phase from XRD patterns is intensely considered as a major advantage. Recombination of the photoinduced e^-/h^+ pairs was considered as the negative effect on the photocatalytic activity of H_2 evolution of the amorphous phase calcined at 500 °C.

In addition, the phase transformation of the TiO_2 photocatalysts occurred beyond the calcinations temperature of 600 °C.

Sreethawong *et al.*, (2005) studied the enhanced photocatalytic hydrogen evolution over Pt supported on mesoporous TiO_2 prepared by single-step sol-gel process (SSSG), in which Pt precursor was introduced into the completely hydrolyzed TiO_2 sol prepared with a mesopore-directing surfactant template. SSSG was utilized to load the Pt cocatalyst onto the systhesized mesoporous TiO_2. For comparative studies, incipient wetness impregnation (IWI), and photo chemical

deposition (PCD) were used to load Pt onto the mesoporous TiO_2 support prepared by the same sol-gel method. The photocatalytic H2 evolution activity of the mesoporous TiO_2 photocatalyst in comparison with Degussa P-25 TiO_2 with various platinum contents was tested systematically. From the result, The SSSG photocatalyst provided the superior photocatalytic activity over the entire range of Pt loading amounts to the other two conventional methods. The enhancement of the photocatalytic activity for H_2 evolution over the largest surface area SSSG photocatalyst may be due to at least 2 possibilities: (1) the increased accessibility of reactant, water molecule, to the photocatalyst surface active sites existing along the mesopore network and (2) the high dispersion of Pt particles deposited through the mesopore structure of TiO_2 support, leading to the better electronic interaction between the cocatalyst and support in the system.

2.4 Photochemical Deposition (PCD)

The morphology of metal particles affects the specific activity of catalysts. A suitable size of metal clusters and higher dispersion for a metal loading are preferred for the catalytic activity. The smaller metal particles are, the larger fraction of the metal atoms exposed at surfaces, where they are accessible to reactant molecules and available for catalysis. (Zhang *et al.*, 2004)

Traditionally, supported metal catalysts are normally prepared by impregnation of high-area support with an aqueous solution of a metal salt. The resultant metal particles on support are usually heterogeneously dispersed with broad size distribution, and some metals cannot deposit onto the surface of support. There are many new techniques have been developed to improve the dispersion of metal particles and control the size distribution of metal particles on support.

One of the attractive techniques is photochemical deposition (PCD) that is the simple method which can be performed at room temperature without introducing any foreign reducing agent.

Photochemical deposition has been used since the early 1960's. Generally, it is similar to "electrodeposition" that is the older, well established material deposition technique. Photochemical deposition is nowadays gaining importance as

an alternative method for preparing heterogeneous catalysts. This technique is obtained by photoelectronic excitation of atoms using light sources as compared to electrochemistry, which uses electrical sources for chemical deposition. It allows metal deposition over semiconductor materials, with simultaneous reduction of metal ions by the electrons of the conduction band. This process can be enhanced by addition of "sacrificial electron donors" e.g. formaldehyde, methanol or 2-propanol that can supply an almost unlimited amount of electrons. PCD takes place at, or near, the photoexcited sites, leading to an enhanced dispersion. (Carabineiro *et al.*, 2010)

In 2000, Sano *et al.* studied on photocatalytic decomposition of N_2O on highly dispersed Ag^+ ions on TiO_2 prepared by photodeposition. Ag-loaded TiO_2 photocatalysts (Ag-TiO_2) in this research were prepared by photodeposition, deposition-precipitation, and impregnation methods. Anatase type TiO_2 (Degussa P-25) was dispersed into $AgNO_3$ solution. The suspension was irradiated by UV light from a high-pressure Hg lamp (Ushio, USH-500D, 500 W) through a longpass filter (cut-off wavelength 295 nm) for 30 min while N_2 gas was passed through the suspension. Amount of Ag loaded on TiO_2 was determined by XRF. From the TEM photograph of Ag-TiO_2 catalyst prepared by photodeposition method in the Figure 2.12, not only no significant changes on TiO_2 surface were observed but the photograph was also almost similar to that of the initial material (TiO_2, P-25) at low Ag loading (0.20 wt%). At higher Ag loading (2.00 wt%), small particles of Ag with a diameter of 1–2 nm were noticeable. This may be due to the aggregation Ag in the photodeposition process when large amount of Ag is photodeposited. Although there is the aggregation observed in case of Ag-TiO_2 catalyst prepared by photodeposition method at higher Ag loading, the aggregation of Ag is more obvious on the photocatalysts prepared by both deposition–precipitation and impregnation methods at only 0.10 wt% Ag loading.

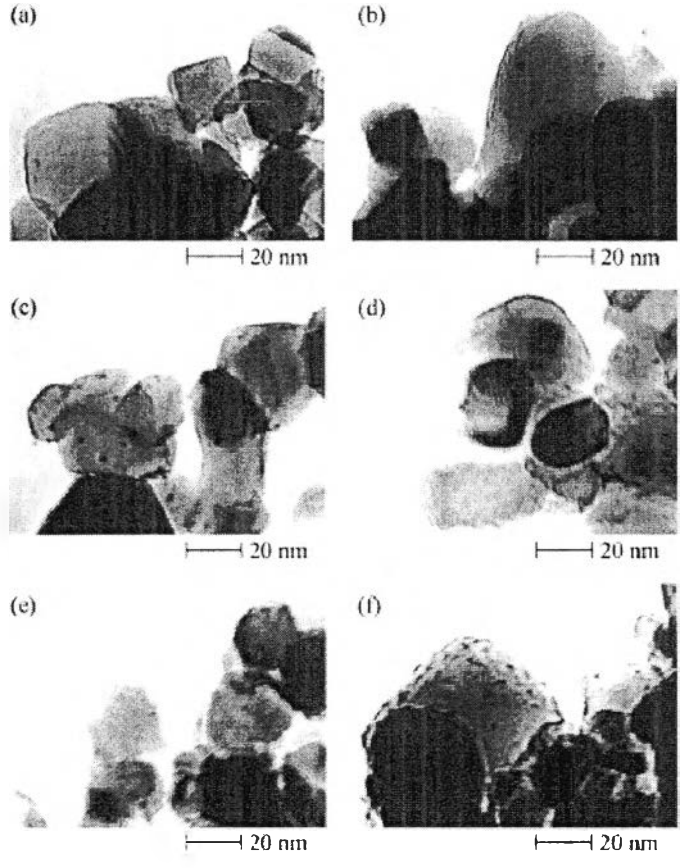

Figure 2.12 TEM photographs of Ag-TiO_2 prepared by (a,b) photodeposition, (c,d) deposition–precipitation, and (e,f) impregnation methods. (a) 0.20 wt% , (b) 2.00 wt% , (c) and (e) 0.10 wt% , (d) and (f) 1.00 wt% (Sano *et al.*, 2000)

In addition, from the results of XPS of Ag-TiO_2 catalyst prepared at low loading (0.20 wt% for photodeposition and 0.10 wt% for both deposition–precipitation and impregnation), larger amount of Ag exists on the surface of catalyst prepared by photodeposition than on the surface of catalyst prepared by the other methods. However, the aggregation of Ag is not confirmed on catalyst prepared by photodeposition. Therefore, Ag particles on the catalyst prepared by photodeposition are highly dispersed when compared with those on the catalyst prepared by the other methods. When compare with the TEM results, The amount of Ag particles observed on catalyst prepared by photodeposition at 2.00 wt% loading is not so different from that on catalyst prepared by deposition–precipitation (both 1.00 and 0.10 wt%) , while the Ag peak intensity in XPS spectrum for the former is larger than that of the latters. The result suggests that a large proportion of the Ag species was well

dispersed on catalyst prepared by photodeposition and a small proportion of the Ag species aggregated on the surface.

Zhang *et al.* (2004) studied on the simple and low cost preparation method for highly dispersed Pd/TiO_2 catalyst. Photochemical deposition was chosen in Pd/TiO_2 catalyst preparation by using sodium tetrachloropalladate(II) (Na_2PdCl_4) as the precursor of palladium ions and TiO_2 (Degussa P-25 with anatase/rutile crystalline ratio of 8:2 and surface area of 50 m^2/g) as the support. The suspention of TiO_2 in Na_2PdCl_4 solution was irradiated with 250W high-pressure mercury light with main wavelength of 365 nm around 6 h. The samples were characterized by AAS, TEM, XRD and XPS. The main objective in this research is to investigate the pH effect on the morphology of deposited palladium. The results of AAS analysis show that the photochemical deposition of palladium ions is nearly 100% to the completion after 6 h irradiation in all cases. The metallic state of the coated palladium particles on TiO_2 support was confirmed from the XPS results. In addition, the XRD and TEM results revealed that Pd/TiO_2 catalyst prepared in the pH region of 6-8 showed the highest average size of palladium particles when compared with other pH region (pH<6, pH 8-10, pH 10-12 and pH 12-13) due to aggregation. Most of palladium particles prepared in the pH region of 6–8 that close to the identical electric point of TiO_2 (IEP of TiO_2 = 6.25) leading to the aggregation of TiO_2 particles, are large and typically polydispersed. The TEM photographs showed in Figure 2.13.

To clearly understand, they showed the deposition mechanism in photochemical deposition according to the following pathway.

$$TiO_2 + h\nu \longrightarrow e^- + p^+ \ (h\nu > E_{bg})$$

$$H_2O \longleftrightarrow H^+ + OH^-$$

$$OH^- + p^+ \longrightarrow OH^0 \longrightarrow \tfrac{1}{2}H_2O + \tfrac{1}{4}O_2\,(g)$$

$$PdCl_4^{2-} + 2e^- \longrightarrow Pd^0 + 4Cl^-$$

$$mPd^0 \longrightarrow Pd_m$$

The overall results of this research demonstrated that homogeneously dispersed palladium particles with sharp size distribution on titanium dioxide could be prepared in the basic solution of 10–13. They also suggested that TiO_2 particles must be stable and well dispersed in the solution to allow their surfaces to completely expose to metal ions, otherwise the adsorption and deposition of metal ions onto those covered surfaces will become impossible.

Photochemical deposition is also used with tubular TiO_2 support (nanotube). Zhu *et al.* (2007) studied on synthesis and catalytic performance of gold-loaded TiO_2 nanofibers. The suspension of TiO_2 nanotubes in $HAuCl_4$ solution used as a gold precursor was irradiated for 6 h by using a 300W High-Pressure Mercury Lamp at a distance of 10 cm under stirring at ambient temperature. In 2008, they also studied on the preparation of palladium-modified TiO_2 nanofibers and their photocatalytic performance. The suspension of TiO_2 nanotubes in $PdCl_2$ solution used as a palladium precursor was irradiated for 3 h by using the same light source and conditions. The results of these researches showed that during the photodecomposition process, the formation of metal particles occurs with the modification of the titanate nanotubular structure and formation of anatase phase. This process can also prevent the formed palladium particles from agglomeration. Therefore, small palladium particles form.

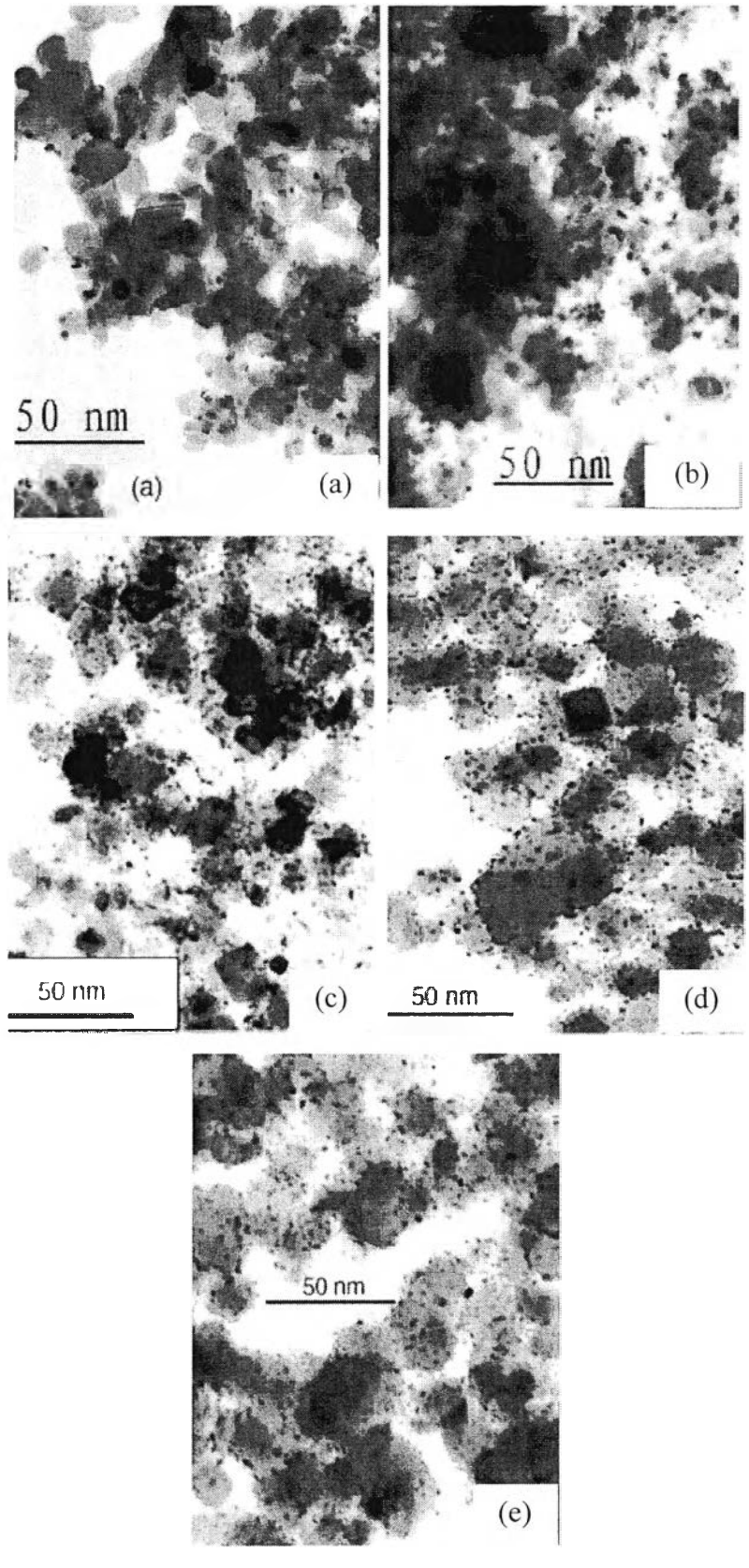

Figure 2.13 TEM images of Pd/TiO_2 particles prepared at: (a) pH < 6 (b) pH = 6–8 (c) pH = 8–10 (d) pH = 10–12 (e) pH = 12–13 (Zhu *et al.*, 2007)

In 2008, Behnajady *et al.* studied on enhancement of photocatalytic activity of TiO_2 nanoparticles by silver doping. They focused on silver doped TiO_2 nanoparticles prepared by liquid impregnation (LI) and photodeposition (PD) methods and characterized by surface analytical methods such as scanning electron micrographs (SEM) and X-ray diffraction (XRD). This catalyst was used in degradation of C.I. Acid Red 88 (AR88) used as a model pollutant from textile industry. In photodeposition, the suspension of TiO_2 in $AgNO_3$ solution was irradiated with UV light (30 W, UV-C, λmax = 254 nm) for 3 h. The result showed that show the AR88 decolorization activity of Ag-photodeopsited TiO_2 was much higher than of silver loaded TiO_2 prepared by LI method. The difference in the photoactivity of Ag/TiO_2 catalyst prepared with different methods can be discussed in terms of the oxidation state of silver on TiO_2 surface. During the preparation process by PD method, Ag^+ ions in the suspension were reduced to Ag, on the other hand, in the LI method silver deposited at TiO_2 surface as Ag^+ ions. Since the electron scavenging by the oxygen at the surface of the excited semiconductor particle cannot efficiently compete with the electron transfer to the silver ion, the electron transfer to silver ion is a rather fast comparing to electron transfer to oxygen molecule and the formation of O_2^- is reduced.

The mesoporous-assembled TiO_2-ZrO_2 mixed oxide nanocrystal photocatalysts synthesized via a modified sol-gel process with the aid of structure-directing surfactant was studied by Onsuratoom *et al.* in 2011. The purpose of the work was to investigate the effect of composition of mesoporous-assembled TiO_2-ZrO_2 mixed oxide nanocrystals on the photocatalytic activity for hydrogen production from the water splitting under UV light irradiation. Tetraisopropyl orthotitanate (TIPT, $Ti(OCH(CH_3)_2)_4$), zirconium (IV) butoxide (ZRB, $Zr(O(CH_2)_3CH_3)_4$ were used as Ti and Zr precursors. Moreover, LAHC and ACA were also used as the same function in synthesis of the nanocrystalline mesoporous titania via a combined sol–gel process with surfactant-assisted templating method (SATM) (Sreethawong *et al.*, Sukulkhaemaruethai *et al.*, 2004). After TiO_2-ZrO_2 mixed oxide was prepared, it was first dispersed in a 50 vol.% aqueous methanol solution, ultrasonicated in order to achieve completely wet photocatalyst surface, and transferred to a photoreactor. Subsequently, $AgNO_3$ aqueous solution was added to

the solution. The mixture was magnetically stirred and irradiated for 2 h by a set of low-pressure Hg lamps (16 lamps, TUV 11 W PL-S, Phillip). After the irradiation, the Ag-deposited TiO_2-ZrO_2 mixed oxide powders were recovered from the solution by filtration, washed with hot distilled water for several times, and dried at 80 °C prior to use.